RSC Advances

ROYAL SOCIETY OF CHEMISTRY

www.rsc.org/advances

Combined spectroscopy and cyclic voltammetry investigates the interaction between [(η^6-*p*-cymene)Ru(benzaldehyde-*N*(4)-phenylthiosemicarbazone)Cl]Cl anticancer drug and human serum albumin

Shan Huang[a,b], Fawei Zhu[a], Qi Xiao[a,b,c,*], Quan Zhou[a], Wei Su[a,], Hangna Qiu[a], Baoqing Hu[b], Jiarong Sheng[a] and Chusheng Huang[a]**

[a] *College of Chemistry and Materials Science, Guangxi Teachers Education University, Nanning 530001, P. R. China*

[b] *Key Laboratory of Beibu Gulf Environment Change and Resources Utilization (Guangxi Teachers Education University), Ministry of Education, China*

[c] *The State Key Laboratory of Virology, Wuhan University, China*

* Corresponding author. Tel.: +86 771 3908065; Fax: +86 771 3908065;

E-mail address: qi.xiao@whu.edu.cn

** Corresponding author. Tel.: +86 771 3908065; Fax: +86 771 3908065;

E-mail address: aaasuwei@yahoo.com.cn

Abstract: In this article, the interaction between [(η^6-*p*-cymene)Ru(benzaldehyde-*N*(4)-phenylthiosemicarbazone)Cl]Cl anticancer drug and human serum albumin (HSA) was investigated systematically under the physiological conditions by using some spectroscopic methods (UV-vis absorption spectroscopy, fluorescence spectroscopy, FT-IR spectroscopy, CD spectroscopy), mass spectroscopy and cyclic voltammetry. The experimental results indicated that this anticancer drug could quench the intrinsic fluorescence of HSA through static quenching mechanism. The Stern-Volmer quenching model has been successfully applied, and the Stern-Volmer quenching constants together with the modified Stern-Volmer quenching constants at different temperatures were also calculated. The corresponding thermodynamic parameters ΔH, ΔG and ΔS were also calculated. The binding of this anticancer drug and HSA resulted in the formation of drug–HSA complex, and the electrostatic interaction played a major role in the complex stabilization. The distance r between the donor (HSA) and the acceptor (drug) was obtained through fluorescence resonance energy transfer theory. Competitive experiments indicated that the binding site of this anticancer drug to HSA was located at site I. The results of synchronous fluorescence spectra, three-dimensional fluorescence spectra, FT-IR spectra and CD spectra indicated that the microenvironment and the conformation of HSA were changed observably at the present of this anticancer drug. The results of mass spectra and cyclic voltammetry further confirmed the interaction between HSA and this anticancer drug. These results indicated that the biological activity of HSA was affected by [(η^6-*p*-cymene)Ru(benzaldehyde-*N*(4)-phenylthiosemicarbazone)Cl]Cl anticancer drug dramatically.

Keywords: Ruthenium anticancer drug, Human serum albumin, Spectroscopy, Cyclic voltammetry, Interaction

1. Introduction

As a kind of organometallic compounds, ruthenium(II) arene complexes of thiosemicarbazone (TSC) with the half-sandwich type structure have attracted great attention by biochemists because of their super-high antibacterial, antiviral and anticancer activities.[1–4] Due to their higher anticancer activity and lower toxicity than platinum drugs, ruthenium(II) arene complexes of TSC anticancer drugs have been widely researched by chemists and medical scientists, and have progressed into potential anticancer drugs in the near future. Until now, some researches have demonstrated the cytotoxicity and the anticancer activity of these ruthenium(II) arene complexes of TSC anticancer drugs. Beckford et al. reported the first structurally characterized ruthenium arene complexes with TSC ligands and further confirmed the good cytotoxic profiles of them against different human cancer cell lines.[5,6] Smith and co-workers demonstrated the cytotoxicity and antiparasitic activity of some mono- and dinuclear ruthenium(II)-arene complexes with TSCs derivatives,[7,8] and Gambino et al. also demonstrated the cytotoxic activities of some organometallic binuclear TSC ruthenium arene complexes.[9,10] More recently, Su's group have synthesized a series of ruthenium(II) arene complexes with TSCs ligands and further investigated their anticancer activities.[11,12] Their results indicated that one of the derivatives of ruthenium(II) arene complexes of TSC anticancer drugs {[(η^6-*p*-cymene)Ru(benzaldehyde-*N*(4)-phenylthiosemicarbazone)Cl]Cl} (structure shown in Fig. 1) was regarded as the potential new anticancer drug with IC_{50} values less than 3.4×10^{-5} mol L^{-1} for human cancer cell lines, which brought its further wide field of application in biomedicine.

Since ruthenium(II) arene complexes of TSC anticancer drugs could intercalate into the structure of nucleic acids, which might inhibit the biological functions of nucleic acids and cause the death of cancer cells,[13–15] DNA or RNA has been demonstrated as the biological targets of these ruthenium(II) arene complexes of TSC anticancer drugs. But beyond that, as the assured potential of ruthenium(II) arene complexes of TSC anticancer drugs in therapy, their absorption, distribution, metabolism and excretion properties in organism are still unknown right now. So, a deeper understanding of their distinct modes of action and improving their selectivity, along with broadening their biomedical application remain the focus of active research.

The investigation of the interactions between ruthenium(II) arene complexes of TSC anticancer

drugs and some important biomolecules became an effective approach for better understanding the mechanism of their anticancer activities, as well as the targeted design and synthesis of new efficient anticancer drugs. However, the research of the interaction between ruthenium(II) arene complexes of TSC anticancer drugs and serum albumin are rarely involved. As a kind of important biomolecules and the principal extracellular soluble protein during the circulatory system, serum albumin, which contributes significantly to the transportation, distribution and metabolism of drugs, is usually chosen as the model protein for the investigation of the interaction between some exogenous ligands and important biomolecules.[16–20] Herein, due to the well-known spatial structures of human serum albumin (HSA),[21–23] HSA was usually used as a model protein for the research of the interactions between exogenous ligands and serum albumin, including the interactions of different drugs and HSA.[24–26]

In this article, the spectroscopic and electrochemical investigations of the interactions between [(η^6-*p*-cymene)Ru(benzaldehyde-*N*(4)-phenylthiosemicarbazone)Cl]Cl anticancer drug and HSA under physiological condition was reported. The interactions of this anticancer drug and HSA were systematically investigated through multispectroscopic approaches and cyclic voltammetry. The intrinsic fluorescence of HSA was quenched dramatically by this anticancer drug by a concentration-dependent manner. The Stern-Volmer quenching constants were decreased with the increase of the temperature, which proved that this anticancer drug could quench the intrinsic fluorescence of HSA effectively through static quenching mechanism. Some thermodynamic parameters, such as ΔH, ΔG and ΔS, were also calculated from both the modified Stern-Volmer equation and the corresponding quenching constants. The distance between this anticancer drug and HSA was calculated through the fluorescence resonance energy transfer (FRET) theory, and the binding site of this anticancer drug to HSA was further investigated. In addition, the microenvironmental and the conformational changes of HSA induced by this anticancer drug were analyzed through the synchronous fluorescence spectroscopy, three-dimensional fluorescence spectroscopy, FT-IR spectroscopy and CD spectroscopy. The binding number and the interaction constant between this anticancer drug and HSA were confirmed by mass spectra and cyclic voltammetry, respectively. This research could provide valuable information of biological action of this anticancer drug in organism, and might serve as important strategy for pharmacological and toxicological research of novel ruthenium(II) arene complexes with TSC anticancer drugs.

2. Materials and methods

2.1 Apparatus

The fluorescence spectra and intensities were performed on Perkin-Elmer LS-55 luminescence spectrometer (PerkinElmer, Waltham, MA, USA) equipped with a 20KW xenon discharge lamp as light source and a thermostatic bath (DKB-501S, Shanghai Jing Hong Laboratory Instrument Co. Ltd, China). The UV-vis absorption spectra were measured on a TU-1901 UV-vis spectrophotometer at room temperature (Beijing Purkinje General Instrument Co., Ltd., Beijing, China). Quartz cells (1 cm path-length) were used for all measurements. The FT-IR spectra were recorded at room temperature on Nicolet iS10 spectrometer (Thermo, USA) equipped with a zinc selenide (ZnSe) attenuated total reflection (ATR) accessory, a deuterated triglycine sulfate (DTGS) detector, and a KBr beam splitter. The CD spectra were recorded on Jasco J-810 automatic recording CD spectropolarimeter (Jasco, Tokyo, Japan) using a cuvette with 1.0 cm path length. The mass spectra were recorded on ACQUITY UPLC/XEVO G2 Q TOF mass spectrometer (Waters Corporation, Milford, USA) equipped with an electrospray ionization probe. The cyclic voltammetric experiments were performed on a CHI-660E electrochemical workstation (Chenhua Instruments Inc., Shanghai, China) with a conventional three-electrode electrochemical testing system. The working electrode was a bare gold electrode (2 mm diameter), whereas the Ag/AgCl electrode served as the reference electrode and a platinum wire was used as the counter electrode. All pH measurements were made with a basic pH meter PB-10 (Sartorius Scientific Instruments Co., Ltd., Beijing, China).

2.2 Materials

The ruthenium(II) arene complexes with TSC [(η^6-*p*-cymene)Ru(benzaldehyde-*N*(4)-phenylthiosemicarbazone)Cl]Cl anticancer drug was synthesized and characterized according to the literature reported before.[11] The structure of this anticancer drug was shown in Fig. 1. The stock solution of 1.0×10^{-3} mol L^{-1} drug was prepared by dissolving its crystals in DMSO. HSA (Sigma, St. Louis, MO, USA) was dissolved in PBS (0.1 mol L^{-1}, pH 7.4) and stored at 4ºC. The concentration of HSA was determined spectrophotometrically using an extinction coefficient ε_{280nm} = 36 600 L mol^{-1} cm^{-1}.[27] The stock

solutions (1.0×10^{-3} mol L^{-1}) of Warfarin (Sigma, St. Louis, MO, USA) and ibuprofen (Sigma, St. Louis, MO, USA) were prepared by dissolving the accurately weighed appropriate amounts of each compound and dissolving in ultrapure water. Then, the solution was diluted to the required volume with ultrapure water in practical use. Ultrapure water with a resistivity of 18.2 MΩ cm was produced by passing through a RiOs 8 unit followed by a Millipore-Q Academic purification set (Millipore, Bedford, MA, USA) and used throughout the whole experiments. All other reagents were of analytical reagent grade and used as received without further purification.

2.3 Fluorescence spectra measurements

Steady-state fluorescence spectra of HSA (2.0×10^{-6} mol L^{-1}) and HSA (2.0×10^{-6} mol L^{-1}) at the present of this anticancer drug ($0 \sim 1.0 \times 10^{-6}$ mol L^{-1}, with an interval of 1.0×10^{-7} mol L^{-1}) were recorded at 298 K, 304 K, 310 K in the wavelength range of 300 ~ 450 nm. The width of the excitation and the emission slit was set to 5.0 nm and 5.0 nm, and the excitation wavelength of 295 nm was chosen in the experiment to avoid inner filter effect. Titrations were performed manually by using trace syringes and each spectrum was the average of three scans.

The binding site investigation experiments were performed by using different site-specific probes (warfarin and ibuprofen for site I and site II on HSA, respectively) through keeping the concentrations of both HSA and site-specific probe constant but varying the concentration of this anticancer drug alone. The steady-state fluorescence spectra of the system were recorded and the corresponding binding constants values of drug–HSA–probe system were evaluated, which could decide the binding site of this specific drug. The concentrations of the site-specific probes and HSA were all 2.0×10^{-6} mol L^{-1}.

The effects of common ions on the binding constant were investigated by recording the steady-state fluorescence spectra of drug–HSA system in the presence of some common metal ions, for example, Ag^{+}, K^{+}, Na^{+}, Cu^{2+}, Zn^{2+}, Ca^{2+}, Mg^{2+}, Ni^{2+}, Co^{2+}, NO_3^{-}, SO_4^{2-} and Cl^{-} at 298 K upon the excitation wavelength at 295 nm. The concentrations of the adopted metal ions and HSA were all 2.0×10^{-6} mol L^{-1}.

The synchronous fluorescence spectra of HSA alone and the drug–HSA system were scanned from 280 ~ 330 nm and 300 ~ 380 nm at the constant $\Delta\lambda$ ($\Delta\lambda = \lambda_{em} - \lambda_{ex}$) of 15 nm and 60 nm, respectively. The $\Delta\lambda$ of 15 nm and 60 nm reflected the spectrum characteristics of tyrosine (Tyr)

and tryptophan (Trp) residues of HSA were observed. The concentration of HSA was kept at 2.0 × 10^{-6} mol L^{-1}.

The three-dimensional fluorescence spectra of HSA alone and the drug–HSA system were performed with the emission wavelength range was 200 ~ 500 nm and the excitation wavelength range was 200 ~ 350 nm with increment of 5 nm. Other scanning parameters were just the same as that of the steady-state fluorescence spectra. The concentrations of HSA and anticancer drug were 2.0 × 10^{-6} mol L^{-1} and 1.0 × 10^{-6} mol L^{-1}, respectively.

2.4 UV-vis absorbance measurements

The UV-vis absorption spectra of free HSA (2.0 × 10^{-6} mol L^{-1}), anticancer drug alone (2.0 × 10^{-6} mol L^{-1}) as well as the drug–HSA system (equal molar ratio) were measured from 200 nm to 350 nm. The solutions of the blank buffer and sample were placed in the reference and sample cuvettes, respectively.

2.5 FT-IR spectra measurements

The FT-IR spectra of free HSA and drug–HSA system in PBS were recorded in the range of 1450 ~ 1800 cm^{-1} with 128 interferograms to ensure a good signal-to-noise ratio. The corresponding absorbance contributions of buffer and free anticancer drug solutions were recorded and digitally subtracted with the same instrumental parameters. All spectra were taken via the ATR method with a resolution of 4 cm^{-1}. The subtraction of the reference spectrum from the spectrum of the protein solution was carried out in accord with the criteria that a straight baseline was obtained between 2000 and 1750 cm^{-1}.[28] The concentration of the anticancer drug was equal to HSA in the FT-IR study.

2.6 CD spectra measurements

For the CD experiment, the concentration of HSA was kept at 2.0 × 10^{-6} mol L^{-1}, while the concentration of anticancer drug was changed from 0 to 1.4 × 10^{-5} mol L^{-1}. The CD spectra were recorded from 200 to 260 nm in 0.1 M PBS (pH 7.4) at room temperature under constant nitrogen flush. The CD profiles were obtained employing a scan speed of 500 nm/min and response time of 0.5 s. Each spectrum was the average of three successive scans and was corrected by PBS buffer solution. Appropriate baseline corrections in the CD spectra were made. The contents of secondary

conformation of HSA (α-helix, β-strand, turn and unordered) were analyzed from CD spectroscopic data.

2.7 Mass spectra measurements

The UPLC was directly interfaced with a Waters XEVO G2 Q TOF mass system equipped with an electrospray ion source operating in either positive or negative ESI mode. Chromatographic separation was achieved on ACQUITY UPLC BEH300 C4 column (1.7 μm, 2.1 × 100 mm) at 80 °C. The mobile phase consisted of a constant flow rate gradient of methanol 0.1% formic acid in water and 0.1% formic acid in acetonitrile under an elution program at a flow rate of 0.2 mL min^{-1}. The analysis run time was 12 min for each injection and the injection volume was 10 μL. The optimal conditions of analysis were as follows: ESI^+ mode, capillary voltage of 2.5 kV, sampling cone voltage was 30.0 V, extraction cone voltage was 4.0 V. The temperature was set at 100 °C, desolvation gas temperature was 350 °C and desolvation gas flow was 800 L h^{-1}. The mass spectrometer was calibrated using a solution of sodium formate before the experiment. The full-scan mass spectral data were produced across the mass range of 500 ~ 4000 Da. Scans were of 12 min duration. Data were collected in centroid mode and mass was corrected during acquisition using an external reference (Lock-Spray) comprising a 200 pg mL^{-1} solution of leucine-enkephalin via a lockspray interface, generating a reference ion at 556.277 Da ($[M + H]^+$) for positive ESI mode.

For these experiments, the HSA concentration was fixed at 2.0×10^{-4} mol L^{-1} and the anticancer drug concentration at 3.0×10^{-3} mol L^{-1}. Free HSA and drug–HSA (molar ratio of 1:1 and 2:1) system were prepared in 0.1% formic acid in acetonitrile and introduced into the mass spectrometer source with a syringe pump. The mass spectral data of all determined samples were further processed by BiopharmLynx V1.3.3 software (Waters Corporation, Milford, USA) for peak detection and peak alignment. The method parameters for data processing were set as follows: retention time range 4.55 ~ 8 min, deconvolution *m*/*z* range 1190 ~ 1480 Da, protein molecular mass range 62000 ~ 75000 Da, mass tolerance 100 ppm, noise elimination level 6 and peak intensity threshold 50.

2.8 Cyclic voltammetry measurements

The bare gold electrode was successively polished by α-Al_2O_3 powder with the diameter of 1.0 μm, 0.3 μm and 0.05 μm, respectively. Subsequently, the bare gold electrode was ultrasonically cleaned in acetone, 0.5 M H_2SO_4 solution and ultrapure water, and then dried by nitrogen airflow. Then, 5 μL HSA solution (2.0×10^{-6} mol L^{-1}) was dropped to the surface of the bare gold electrode. After 6 h, the electrode was washed by ultrapure water several times and dried in nitrogen airflow and was then ready for use. All three of the electrodes were fixed by the O-ring onto a panel constructed from virgin Teflon. The electrolyte used in the experiments was a solution of 1:1 5.0×10^{-3} mol L^{-1} $K_3Fe(CN)_6/K_4Fe(CN)_6$, and 10 mL of electrolyte was added into an electrochemical cell with a magnetic stirring device. After that, different amounts of the anticancer drug solution were added continuously to the system and stirred for 5 min; then, the system was at rest for 3 min before testing. The cyclic voltammograms of HSA modified gold electrode in the absence and the presence of drug were recorded at a scan rate of 50 mV s^{-1}, with the concentration of anticancer drug varied from 1.2×10^{-7} mol L^{-1} to 9.6×10^{-7} mol L^{-1}. All measurements were repeated three times with different electrodes at room temperature.

3. Results and discussion

3.1 Fluorescence quenching investigation

It is well-know that the intrinsic fluorescence of HSA is mostly contributed by Try residue alone and is very sensitive to its local microenvironment. The interaction of other molecules and HSA could result in the intrinsic fluorescence quenching of HSA obviously.[29] The fluorescence quenching is mainly occurred by collisional process (dynamic quenching) and/or ground state complex formation by quencher and fluorophore (static quenching). Since the steady-state fluorescence spectroscopy is widely used to obtain the local information about both microenvironmental and conformational changes of fluorophore,[30,31] which can further confirm the fluorescence quenching mechanism. So, the fluorescence spectra of HSA with different concentrations of [(η^6-*p*-cymene)Ru(benzaldehyde-*N*(4)-phenylthiosemicarbazone)Cl]Cl anticancer drug were recorded by the steady-state fluorescence spectroscopy, which was in order to know whether drug formed a complex with HSA or just collided with HSA by accident.

The effect of this anticancer drug on the fluorescence intensity of HSA at 298 K was shown in Fig. 1. It could be seen that HSA showed a strong fluorescence emission band around 350 nm in

the wavelength range of 300 ~ 450 nm and under the excitation wavelength of 295 nm, while the anticancer drug showed almost no fluorescence emission in the same conditions (line L in Fig. 1). Furthermore, the fluorescence intensity of HSA was quenched regularly with the increase of the anticancer drug concentration, and the fluorescence intensity of HSA decreased dramatically when the anticancer drug with higher concentration was present in the solution, which suggested that the anticancer drug could interact with HSA and then quench the intrinsic fluorescence of HSA by concentration-dependent manner.[22,23] Same trends could also be observed at other temperatures (304 K and 310 K), but the fluorescence emission positions and the shapes of fluorescence spectra were almost not changed in the whole process.

3.2 Fluorescence quenching mechanism

The possible fluorescence quenching mechanism might be either static or dynamic or both of them that could be distinguished easily by the difference on temperature dependence. The quenching constants decrease with the increment of temperature for static quenching while the reverse is true for dynamic quenching. Since the fluorescence quenching data at different temperature are plotted as the relative fluorescence intensity of HSA versus the anticancer drug concentration, the quenching constants of different temperature can be calculated through the well-known Stern-Volmer equation shown below:[32]

$$\frac{F_0}{F} = 1 + k_q \tau_0 [Q] = 1 + K_{SV} [Q] \qquad (1)$$

In the above equation, F_0 and F represent the steady-state fluorescence intensities of fluorophore at the absent and present of quencher, respectively. k_q is the bimolecular quenching constant and the maximum value of k_q is 2.0×10^{10} L mol^{-1} s^{-1} for dynamic quenching, τ_0 is the fluorescent lifetime of fluorophore in the absence of quencher and τ_0 is approximately 1.0×10^{-8} s for HSA. K_{SV} is the Stern-Volmer quenching constant and [Q] is the concentration of quencher. So, the Stern-Volmer quenching constant K_{SV} value can be calculated by the linear regression of a plot of F_0 / F against [Q], and k_q value can be calculated by the ratio of K_{SV} / τ_0 from the above equation.

In order to evaluate the dilution effect by buffer solutions, the measurement of HSA titrated by buffer was performed. It was observed that the fluorescence spectra of HSA were almost not varied during the buffer titration process. The plots of Stern-Volmer equation at different

temperature were shown in Fig. 2A, and the values of Stern-Volmer quenching constants K_{SV} and bimolecular quenching constants k_q at three different temperatures were listed in Table 1. As shown in Fig. 2A, the results agreed well with the Stern-Volmer equation at lower concentrations ($0 \sim 1.0 \times 10^{-6}$ mol L^{-1} with an interval of 1.0×10^{-7} mol L^{-1}), since the results could depart from the initial linearity at higher concentrations due to the inner filter effects.[33] Furthermore, as indicated in Table 1 that both the K_{SV} and k_q values increased with the temperature rising, indicating that the probable quenching mechanism of HSA by this anticancer drug could be a dynamic quenching rather than static quenching. However, the k_q values were larger than 2.0×10^{10} L mol^{-1} s^{-1} all (the maximum value for dynamic quenching), suggesting that the quenching mechanism might be a static quenching mechanism.

It is well known that the dynamic quenching can only affect the excited states of fluorophores and no obvious variations in the absorption spectra of fluorophores are expected, so the UV-vis absorption spectra are further performed to identify the real quenching mechanism of this procedure.[34] As shown in Fig. 3, the UV-vis absorption spectrum of HSA (curve B in Fig. 3) in the near ultraviolet band (200 ~ 350 nm) and the difference absorption spectrum between drug–HSA system and anticancer drug alone (curve D in Fig. 3) at the same range could not be superposed within experimental error, indicating the ground state complex formation between this anticancer drug and HSA rather than the dynamic collision. The results could further confirm that the fluorescence quenching mechanism of HSA by this anticancer drug was mainly a static quenching mechanism.

For the static quenching process, the quenching data could be further analyzed according to the modified Stern-Volmer equation:[32]

$$\frac{F_0}{\Delta F} = \frac{1}{f_a K_a [Q]} + \frac{1}{f_a} \qquad (2)$$

In the present case, F_0 is the fluorescence intensity of fluorophore in the absence of quencher, and ΔF is the difference of the fluorescence intensities of fluorophore in the absence and presence of quencher. f_a is the mole fraction of solvent accessible fluorophore, K_a is the effective quenching constant for the accessible fluorophores and $[Q]$ is the concentration of quencher,[35] respectively, which are analogous to associative binding constants for the quencher–acceptor system.[36,37] The dependence of F_0 / ΔF on the reciprocal value of quencher concentration $[Q]^{-1}$ is linear with the

slope equaling the value of $(f_a K_a)^{-1}$, and the value of f_a^{-1} is fixed on the ordinate. The modified Stern-Volmer quenching constant K_a can be calculated from the quotient of the ordinate f_a^{-1} and the slope $(f_a K_a)^{-1}$. The plots of modified Stern-Volmer equation were shown in Fig. 2B, and the corresponding modified Stern-Volmer quenching constants K_a at three different temperatures were also listed in Table 1. The decreasing trend of K_a with increasing temperature indicated that the fluorescence quenching was mainly arisen from static quenching by complex formation.[32]

3.3 The investigation of the interaction between drug and HSA

3.3.1 Binding force

In general, the interactions forces between other exogenous ligands and biological macromolecules may contain van der Waals interactions, hydrophobic force, multiple hydrogen bonds, electrostatic interactions and so on.[38] The interaction force between this anticancer drug and HSA can be elucidated through the variation of the thermodynamic parameters calculated from the van't Hoff plots. If the enthalpy change (ΔH) does not change obviously in the temperature range, both the enthalpy change (ΔH) and the entropy change (ΔS) can be calculated from the van't Hoff equation shown below:

$$\ln K_a = -\frac{\Delta H}{RT} + \frac{\Delta S}{R} \quad (3)$$

where K_a is the same to the associative binding constant at the corresponding temperature and R is the gas constant. As shown in Fig. 4, a good linear relationship between the ln K_a and 1 / T was existed. According to the slopes and the intercepts as shown in Fig. 4, the values of ΔH and ΔS could be calculated and the results were also shown in Table 1. Furthermore, the free energy change (ΔG) can be calculated from the below equation:

$$\Delta G = \Delta H - T\Delta S \quad (4)$$

The values of ΔG at different temperatures were all incorporated in Table 1. The negative values of ΔG and the positive value of ΔS indicated that the binding process of drug to HSA was spontaneous. The negative ΔH and the positive ΔS values of the interactions of drug and HSA suggested that the electrostatic interactions played major roles in this binding reaction,[39] which was agreed well with the conclusion reported before.[40] Moreover, hydrophobic interactions and coordination binding might also participate in the interaction of HSA with this anticancer drug.

3.3.2 Binding constant and binding number

When the small molecules bind independently to the macromolecules with the equivalent sites, the binding constant and the binding number between the small molecules and the macromolecules can be assessed by the following double-logarithmic equation:[41]

$$\log\frac{F_0 - F}{F} = \log K_b + n\log[Q] \quad (5)$$

In the present case, F_0 and F are the fluorescence intensities of fluorophore in the absence and the presence of quencher, respectively. K_b is the binding constant and n is the binding number of the fluorophore and quencher system, which can be abstained by the plot of log $(F_0 - F) / F$ versus log $[Q]$. Table 2 demonstrates the results analyzed by this way for drug–HSA system at different temperatures. It could be seen that the value of K_b increased dramatically with the increase of temperatures, while n was almost kept constant, indicating that this anticancer drug bound strongly with HSA according to mole ratio 1:1, and independent of the binding site for this anticancer drug to HSA.

3.3.3 Effects of common ions on the binding constant

Some common ions distributed in human plasma could affect the interactions of other exogenous ligands and serum albumins, the effects of some common ions (Ag^+, K^+, Na^+, Cu^{2+}, Zn^{2+}, Ca^{2+}, Mg^{2+}, Ni^{2+}, Co^{2+}, NO_3^-, SO_4^{2-} and Cl^-) on the binding constant of drug–HSA system were investigated at 298 K and the corresponding results were summarized in Table 3. It could be seen clearly that the binding constant values of drug–HSA system were decreased at the present of some common ions, which might be due to the competition between this anticancer drug and common ions. This results indicated that the anticancer drug had a short storage time in blood plasma and would be easily cleared from the blood.[22] In the clinical therapy, it is quite necessary to use high doses of anticancer drug to achieve the desired therapeutic effect.[42]

3.3.4 Binding site

The data in preceding discussion could not provide the precise binding sites of drug on HSA, so the competitive displacement experiments were carried out by using warfarin and ibuprofen as site-specific probes.[43,44] As shown in Fig. 5, after the addition of warfarin, the maximum fluorescence emission wavelength of HSA was red-shifted obviously and the fluorescence

intensity of HSA was significantly higher than that of HSA alone. However, if ibuprofen was present, the fluorescence intensity of HSA decreased slightly than that of HSA alone but the maximum fluorescence emission wavelength of HSA was not shifted apparently compared with HSA alone. When the anticancer drug was added into the HSA–probe system, the fluorescence intensity of HSA decreased gradually whether the site-specific probe was warfarin or ibuprofen, but a tiny red shift of the maximum fluorescence emission wavelength of HSA occurred if the site-specific probe was warfarin.

In order to facilitate the comparison of the influence of site-specific probes on the fluorescence quenching of HSA by this anticancer drug, the Stern-Volmer quenching constants of drug–HSA–probe system were further analyzed using the equation (1). The Stern-Volmer quenching constant values at 298 K were noticed to be 4.19×10^5 L mol^{-1}, 1.83×10^5 L mol^{-1} and 3.72×10^5 L mol^{-1} for drug–HSA system, drug–HSA–warfarin system and drug–HSA–ibuprofen system, respectively. As evident from the results, the Stern-Volmer quenching constant was all decreased at the present of warfarin or ibuprofen but it was decreased dramatically at the present of warfarin than ibuprofen, which indicted that this anticancer drug could be significantly displaced by warfarin and the binding site of this anticancer drug was mainly located within site I. Hence, the site I, which has been described as a large hydrophobic cavity present in subdomain IIA of HSA and involved the lone Trp214 residue of HSA,[45] was proposed to be the main binding site for this anticancer drug in HSA. Furthermore, it is reported before that HSA has negative net charge of about −15, while it contains three subdomains with different net charges under the physiological pH: −9 (subdomain I), −8 (subdomain II), and +2 (subdomain III).[46] This anticancer drug in solution was positively charged and could bind to the surface of subdomain I and subdomain II spontaneously, which demonstrated that the electrostatic interaction was the main force in the interaction between HSA and this anticancer drug.

3.4 Energy transfer between HSA and drug

Since HSA contains the lone Trp214 in subdomain IIA, the distance between the binding site of this anticancer drug and the fluorophore (Trp214) of HSA could be calculated according to Förster theory of fluorescence resonance energy transfer (FRET). According to the Förster theory of FRET, both the efficiency of energy transfer (E) and the distance (r) between the donor (Trp214 in

HSA) and the acceptor (drug) could be calculated by the equation shown below:[32]

$$E = 1 - \frac{F}{F_0} = \frac{R_0^6}{R_0^6 + r^6} \quad (6)$$

herein R_0 is the critical distance when E = 50 %, and can be calculated from the below equation:

$$R_0^6 = 8.79 \times 10^{-25} K^2 n^{-4} \phi J \quad (7)$$

In the above equation, K^2 is the space factor of orientation related to the geometry of the donor and the acceptor of dipoles and K^2 = 2/3 for random orientation in solution; n is the refracted index of medium and n = 1.36 usually; ϕ is the fluorescence quantum yield of the donor without the acceptor and ϕ = 0.074 for HSA;[47] J is the degree of spectral overlap between the emission spectrum of the donor and the absorption spectrum of the acceptor (Fig. 6), which can be calculated by the equation:

$$J = \frac{\int_0^\infty F(\lambda)\varepsilon(\lambda)\lambda^4 d\lambda}{\int_0^\infty F(\lambda) d\lambda} \quad (8)$$

Herein, $F(\lambda)$ is the corrected fluorescence intensity of the donor in the wavelength range of λ to $\lambda + \Delta\lambda$; $\varepsilon(\lambda)$ is the extinction coefficient of the acceptor at λ.

According to above equations, the calculated values of R_0 and r were 4.31 nm and 3.68 nm, respectively. The absolute value of the average distance between the donor and the acceptor was in the range of 2 ~ 8 nm and $0.5R_0 < r < 1.5R_0$,[48] indicating the higher probability of occurrence of the energy transfer from HSA to this anticancer drug, which was also in accordance with the electrostatic interaction mechanism.

3.5 Conformation change investigation

3.5.1 Synchronous fluorescence spectroscopy

Synchronous fluorescence spectra can provide some characteristic information about the microenvironment in the vicinity of fluorophore and the sensitivity associated with the synchronous fluorescence is still maintained while offering some advantages: simplification of the spectra, reduction of the spectral bandwidth and avoiding of the perturbing effects.[49] Synchronous fluorescence spectroscopy is usually used to characterize and provide fingerprints of complex samples by simultaneous scanning of the emission and the excitation monochromators with a

constant wavelength difference between them ($\Delta\lambda$). The characteristic information of Tyr residue and Trp residue can be exhibited at the $\Delta\lambda$ = 15 nm and $\Delta\lambda$ = 60 nm,[26] respectively.

The influence of this anticancer drug on the synchronous fluorescence spectrum of HSA applied to the microenvironment investigation of Tyr residue and Trp residue was shown in Fig. 7. It was apparent from Fig. 7 that the maximum emission wavelength of Tyr residue ($\Delta\lambda$ = 15 nm) showed a subtle red shift (from 299 nm to 302 nm), while the maximum emission wavelength of Trp residue ($\Delta\lambda$ = 60 nm) exhibited a tiny blue shift (from 340 nm to 339 nm). These results suggested that the binding of this anticancer drug to HSA could affect the microenvironment around Tyr and Trp,[50] and the Tyr residue became much more hydrophobic while the Trp residue became much more hydrophilic. As shown in Fig. 7C, the curve of $\Delta\lambda$ = 60 nm was lower than that of $\Delta\lambda$ = 15 nm, indicating that Trp residue played an important role during the fluorescence quenching of HSA by this anticancer drug and the anticancer drug could approach the Trp residue more than the Tyr residue.[51]

3.5.2 Three-dimensional fluorescence spectroscopy

The conformation variation of HSA resulted from this anticancer drug could be investigated more carefully through three-dimensional fluorescence spectroscopy. As shown in Fig. 8, four peaks could be seen obviously in three-dimensional fluorescence spectra. Peak a and peak b mainly represented the first-ordered Rayleigh scattering peak ($\lambda_{ex} = \lambda_{em}$) and the second-ordered Rayleigh scattering peak ($\lambda_{em} = 2\lambda_{ex}$), respectively. The intensities of both the first-ordered and the second-ordered Rayleigh scattering peaks increased at the present of the anticancer drug, which might be due to the formation of the drug–HSA complex and the increase of the macromolecule diameter. In addition, two strong fluorescence peaks could be seen in the middle of Fig. 8. Peak 1 ($\lambda_{ex/em}$ = 285.0/346.6 nm) and peak 2 ($\lambda_{ex/em}$ = 230.0/345.9 nm) dominatingly revealed the fluorescence spectral behavior of Trp residue of HSA and the polypeptide backbone structures of HSA, respectively, which were well correlated with their microenvironment's polarity.[31] The results shown in Table 4 indicated that the fluorescence intensity of peak 1 decreased from 627.5 to 438.2 with the addition of this anticancer drug, suggesting that the interaction of this anticancer drug with HSA induced the change of the polar environment of Trp residue.[20] Moreover, the fluorescence intensity of peak 2 decreased rapidly from 614.4 to 158.3 after the addition of this

anticancer drug, indicating that the peptide structure of HSA was changed obviously. The entire phenomenon and the analyzing data proved that the binding of this anticancer drug to HSA resulted in both the great unfolding of the polypeptides of HSA and the slight conformational change of HSA.

3.5.3 FT-IR spectroscopy

FT-IR spectroscopy is another effective method to directly analyze the variation of the secondary structure of proteins under the influence of other exogenous ligands. The FT-IR spectra of proteins exhibit some amide bands, including the amide I band (1600 ~ 1700 cm^{-1}, mainly C=O stretch) and amide II band (1500 ~ 1550 cm^{-1}, C–N stretch coupled with N–H bending mode) both related with the secondary structure of proteins.[22] Compared with the amide II band, the amide I band is more sensitive to the variation of the secondary structure of proteins. The FT-IR spectra of free HSA and drug–HSA system in PBS were shown in Fig. 9. As could be seen from infrared spectrum of free HSA, the peak positions of the amide I band and the amide II band were observed at 1652.5 cm^{-1} and 1548.2 cm^{-1}, respectively. When this anticancer drug was present in HSA solution, the peak position of amide I band moved from 1652.5 cm^{-1} to 1658.1 cm^{-1} and the peak position of amide II band moved from 1548.2 cm^{-1} to 1544.0 cm^{-1}, together with the changes in the peak intensities of both amide I band and amide II band. These results indicated that this anticancer drug could interact with C=O, C–N and N–H groups in the protein polypeptides that resulted in the rearrangement of the secondary structure of HSA.[52]

3.5.4 CD spectroscopy

CD spectroscopy is an effective and quantitative technique to investigate the conformation of proteins in aqueous solution. In order to prove the possible influence of this anticancer drug binding on the secondary structure of HSA, the CD spectroscopy of HSA in the absence and in the presence of different concentration of this anticancer drug was performed. It is well-known that HSA exhibited two negative absorption peaks at about 208 nm and 222 nm which were the characteristic absorption peaks of the α-helical structure of protein and resulted from the $n \rightarrow \pi^*$ transfer for the bond of the α-helix.[22] The CD results can be expressed in terms of the mean residue ellipticity (MRE) according to the following equation:

$$\mathrm{MRE} = \frac{\text{Observed CD(mdeg)}}{C_{\mathrm{p}} n l \times 10} \quad (9)$$

Where, C_{p} is the molar concentration of the protein, l is the path length (1.0 cm), n is the number of amino acid residues and n is 585 for HSA, respectively. The α-helical contents of free HSA and combined HSA can be calculated from MRE values at 208 nm using the following equation:[53]

$$\alpha\text{-helix}(\%) = \frac{-\mathrm{MRE}_{208} - 4000}{33000 - 4000} \times 100 \quad (10)$$

Herein, MRE_{208} is the observed MRE value at 208 nm. 4000 represents the MRE value of the β-form and random coil conformation cross at 208 nm and 33000 means the MRE value of a pure α-helix at 208 nm, respectively. From the above equation, the α-helicity in the secondary structure of HSA could be easily determined.

As shown in Fig. 10, HSA exhibited two negative absorption bands in the far-UV region at 208 nm and 222 nm, which was consistent with the results reported before. However, the CD intensity at 208 nm was decreased dramatically and the shape of the CD spectrum was also changed significantly after the addition of the anticancer drug. In order to quantify the different contents of the secondary structures of HSA, the CD spectra were analyzed by the algorithm SELCON3 and the values of secondary structures for HSA were also calculated. As shown in Table 5, a decreasing tendency of the α-helices content and increasing tendencies of other secondary structure contents were estimated at higher concentration of this anticancer drug. The α-helices content of HSA decreased from 60.1% to 43.4%, while the β-strand content of HSA increased from 6.0% to 8.2% and the unordered content of HSA also increased from 20.1% to 24.8%, when the concentration of this anticancer drug increased from 0 to 1.4×10^{-5} mol L^{-1}, which indicated that the decrease of the biological activity of HSA upon the interaction with this anticancer drug of higher concentration. In addition, the decrease of the α-helices content in the secondary structure of HSA also indicated that this anticancer drug could enter the hydrophobic pocket of HSA and destroyed the hydrogen bonding networks of HSA. These results further elucidated that a stronger structural change of that was related to a low degree of surface coverage.[54]

3.6 Mass spectra investigation

The ground state complexation of exogenous ligands with HSA could be further demonstrated

by using XEVO G2 Q TOF mass spectrometry which was considered to be an accurate and sensitive approach for the verification of the binding interaction between exogenous ligands and HSA.[55] In order to prove the static quenching mechanism between drug and HSA, the mass spectra of free anticancer drug, free HSA and drug–HSA complexes were performed and all depicted in Fig. 11. It was easily to know that the precise molecular mass of anticancer drug was 561.53 according to the molecular formula, but in the positive ion spectrum, the main fragment ion of anticancer drug was observed at *m*/*z* 490 (Fig. 11A) that was corresponded with the molecular mass of the structure of $[M–Cl–HCl]^{+}$.[11]

According to Fig. 11B, it could be seen that the average molecular mass of HSA alone was around 66438 Da, which was in accordance with the reported value.[55] The same molecular mass of 66438 Da could also be seen when the anticancer drug was present (Fig. 11C). Furthermore, after the addition of anticancer drug, new peaks corresponded with different molecular mass occurred at about 66927 Da and 66962 Da, and the molecular mass was increased by 491 Da and 524 Da compared with the molecular mass of HSA alone. Since the molecular weight of the main fragment ion of anticancer drug in the positive ion spectrum was 490 Da, indicating that this anticancer drug was indeed binding to HSA. In addition, the anticancer drug could easily detach a chloride ion and existed in the structure of $[M–Cl]^{+}$ (molecular mass 526 Da) in solution,[56] so the positively-charged anticancer drug could easily bind with the negatively-charged HSA in physiological conditions and then the molecular mass of around 66964 Da appeared spontaneously. These results were a clear indication that the additional molecular mass on HSA originated from one molecule of anticancer drug ligand. Moreover, the same molecular mass could be seen in drug–HSA system with different molecular ratio of anticancer drug versus HSA (Fig. 11C and Fig. 11D), which further revealed that the binding number of anticancer drug to HSA was 1:1 that was consistent with the fluorescent spectrometry result. Thus, this additional molecular mass of one anticancer drug molecule revealed the presence of a single anticancer drug molecule associated with HSA on average.

3.7 Cyclic voltammetry investigation

Cyclic voltammetry is an effective method to directly analyze the interaction between proteins and drugs under the physiological conditions.[16,57] In order to further confirm the results obtained

from the spectroscopic methods, cyclic voltammetry is used to investigate the interaction between this anticancer drug and HSA at gold electrode. Since HSA need to be fixed on the surface of gold electrode, the HSA-modified gold electrode is characterized firstly by using $K_3Fe(CN)_6/K_4Fe(CN)_6$ probe which shows different electrochemical behavior on different films. As indicated in Fig. 12, a good electrochemical response of $K_3Fe(CN)_6/K_4Fe(CN)_6$ with a pair of reversible redox peaks existed on both bare gold electrode and HSA-modified gold electrode. However, the formal redox peak potentials negatively shifted and the formal redox peak currents dramatically decreased, showing the great variation occurred on the surface of the gold electrode. Furthermore, after the modification of HSA on the surface of gold electrode, the separation of redox peak potential increased from 84 mV to 97 mV and the separation of redox peak current decreased from 83.4 μA to 80.7 μA, respectively, indicating the decrease of both the electron-transfer rate of $K_3Fe(CN)_6/K_4Fe(CN)_6$ and the conductivity of the modified gold electrode. In addition, the gold electrode treated with HSA could be reused with the constant redox peak potentials and redox peak currents, demonstrating the immobilization of HSA on the surface of gold electrode.

This HSA-modified gold electrode was subsequently used as the working electrode to investigate the interaction between this anticancer drug and HSA. As shown in Fig. 12, when the anticancer drug was administrated into the $K_3Fe(CN)_6/K_4Fe(CN)_6$ electrolyte solution, a significant decrease in the redox peak currents and a tiny shift in the redox peak potentials were happened. The decrease of the redox peak currents and the shift of the redox peak potentials after the addition of this anticancer drug might result from the interaction between HSA and this anticancer drug that reduced the diffusion coefficient of $K_3Fe(CN)_6/K_4Fe(CN)_6$ subsequently. Furthermore, the lower the redox peak current was generated when the higher the concentration of this anticancer drug was present, which suggested that this anticancer drug could decrease the redox peak currents by concentration-dependent manner. According to values of the redox peak currents in the presence of different concentrations of anticancer drug obtained from Fig. 12, a good linear relationship existed between the reciprocal of the current drop and the reciprocal of the anticancer drug concentration, with a correlation coefficient of 0.998. It was compliance with the Langmuir equation:[57]

$$\frac{1}{\Delta I_p} = \frac{1}{\Delta I_{p\,max}} + \frac{1}{\Delta I_{p\,max} K_a c} \quad (11)$$

Herein, ΔI_p is the current drop, ΔI_{pmax} is the maximum of the current drop, K_a is the binding equilibrium constant between HSA and the anticancer drug, and c is the concentration of the anticancer drug, respectively. According to the equation and the slope of the curve insert in Fig. 12, the value of the equilibrium constant K_a was 1.267×10^5 L mol^{-1}, which was a little lower than the value of the binding constant obtained by spectroscopic methods. Moreover, the electrode was washed with ultrapure water and then dipped into fresh $K_3Fe(CN)_6/K_4Fe(CN)_6$ solution, the redox peak currents changed greatly, suggesting the complex formation between this anticancer drug and HSA on the surface of gold electrode, which was consistent well with the results proved by multispectroscopic approaches.

4. Conclusions

During this work, we systematically investigated the interactions between [(η^6-*p*-cymene)Ru(benzaldehyde-*N*(4)-phenylthiosemicarbazone)Cl]Cl anticancer drug and HSA by UV–vis absorption spectra, fluorescence spectra, FT-IR spectra, CD spectra, mass spectra and cyclic voltammetry under the physiological conditions. The Stern-Volmer quenching constants, the bimolecular quenching constants, the modified Stern-Volmer quenching constants and the binding constants were all obtained. The results indicated that this anticancer drug quenched the intrinsic fluorescence of HSA effectively by concentration-dependent manner, the quenching mainly belonged to the static quenching. The subsequent results indicated that the binding interaction between this anticancer drug and HSA could be affected efficiently by common metal ions. The values of some thermodynamic parameters elucidated that the electrostatic interactions played major roles during their interaction, and this anticancer drug could effectively occupy site I. The Synchronous fluorescence spectroscopy, three-dimensional fluorescence spectroscopy, FT-IR spectroscopy and CD spectra were further used to indicate the microenvironmental and conformational changes of HSA with this anticancer drug, which indicated that the microenvironment and the conformation of HSA were changed drastically at the present of this drug and the biological activity of HSA was weakened in the present of this anticancer drug. The results of mass spectra further demonstrated that the binding number of anticancer drug to HSA

was 1:1. Cyclic voltammetry further confirmed the interaction between HSA and this anticancer drug. These results made a better understanding on the interactions between ruthenium(II) arene complexes of TSC anticancer drug and serum albumin, which is much important for the further applications of this kind of anticancer drug in biomedical and therapeutical fields.

Acknowledgements

This work was financially supported by the National Natural Science Foundation of China (21203035, 21261005, 51263002), the Guangxi Natural Science Foundation (2013GXNSFCA019005, 2013GXNSFBA019029), the Scientific Research Foundation of Guangxi Provincial Education Department (2013YB138, ZD2014081), the Scientific Research Foundation for the Returned Overseas Chinese Scholars, State Education Ministry and Open Research Fund Program of the State Key Laboratory of Virology of China (2014KF006).

References

[1] M. Adams, Y. Q. Li, H. Khot, C. D. Kock, P. J. Smith, K. Land, K. Chibale and G. S. Smith, The synthesis and antiparasitic activity of aryl- and ferrocenyl-derived thiosemicarbazone ruthenium(II)–arene complexes, *Dalton Trans.*, 2013, **42**, 4677–4685.

[2] A. K. Singh, D. S. Pandey, Q. Xu and P. Braunstein, Recent advances in supramolecular and biological aspects of arene ruthenium(II) complexes, *Coordin. Chem. Rev.*, 2014, **270–271**, 31–56.

[3] Q. Zhou, P. Y. Li, R. M. Lu, Q. Q. Qian, X. L. Lei, Q. Xiao, S. Huang, L. F. Liu, C. S. Huang and W. Su, Synthesis, X-ray diffraction study and cytotoxicity of a cationic p-cymene ruthenium chloro complex containing a chelating semicarbazone ligand, *Z. Anorg. Allg. Chem.*, 2013, **639**, 943–946.

[4] L. F. Liu, P. Y. Li, Q. Q. Qian, X. L. Lei, Y. X. Huang, Q. Zhou, S. Huang, Q. Xiao and W. Su, Synthesis, structure, anticancer activity of 2-formylthiophene thiosemicarbazones and their organometallic ruthenium complexes, *Chin. J. Org. Chem.*, 2013, **33**, 854–859.

[5] F. A. Beckford, G. Leblanc, J. Thessing, M. Jr Shaloski, B. J. Frost, L. Li and N. P. Seeram, Organometallic ruthenium complexes with thiosemicarbazone ligands: Synthesis, structure and cytotoxicity of $[(\eta^6\text{-}p\text{-cymene})\text{Ru(NS)Cl}]^+$ (NS = 9-anthraldehyde thiosemicarbazones),

Inorg. Chem. Commun., 2009, **12**, 1094–1098.

[6] F. A. Beckford, D. Dourth, M. Jr. Shaloski, J. Didion, J. Thessing, J. Woods, V. Crowell, N. Gerasimchuk, A. Gonzalez-Sarrías and N. P. Seeram, Half-sandwich ruthenium–arene complexes with thiosemicarbazones: synthesis and biological evaluation of [(η^6-*p*-cymene)Ru(piperonal thiosemicarbazones)Cl]Cl complexes, *J. Inorg. Biochem.*, 2011, **105**, 1019–1029.

[7] T. Stringer, B. Therrien, D. T. Hendricks, H. Guzgay and G. S. Smith, Mono- and dinuclear (η^6-arene) ruthenium(II) benzaldehyde thiosemicarbazone complexes: synthesis, characterization and cytotoxicity, *Inorg. Chem. Commun.*, 2011, **14**, 956–960.

[8] M. Adams, Y. Li, H. Khot, C. De Kock, P. J. Smith, K. Land, K. Chibalea and G. S. Smith, The synthesis and antiparasitic activity of aryl- and ferrocenyl-derived thiosemicarbazone ruthenium(II)-arene complexes, *Dalton Trans.*, 2013, **42**, 4677–4685.

[9] B. Demoro, C. Sarniguet, R. Sanchez-Delgado, M. Rossi, D. Liebowitz, F. Caruso, C. Olea-Azar, V. Moreno, A. Medeiros, M. A. Comini, L. Otero and D. Gambino, New organoruthenium complexes with bioactive thiosemicarbazones as co-ligands: potential anti-trypanosomal agents, *Dalton Trans.*, 2012, **41**, 1534–1543.

[10] B. Demoro, R. F. M. de Almeida, F. Marques, C. P. Matos, L. Otero, J. C. Pessoa, I. Santos, A. Rodríguez, V. Moreno, J. Lorenzo, D. Gambino and A. I. Tomaz, Screening organometallic binuclear thiosemicarbazone ruthenium complexes as potential anti-tumour agents: cytotoxic activity and human serum albumin binding mechanism, *Dalton Trans.*, 2013, **42**, 7131–7146.

[11] W. Su, Q. Zhou, Y. M. Huang, Q. Y. Huang, L. N. Luo, Q. Xiao, S. Huang, C. S. Huang, R. Chen, Q. Q. Qian, L. F. Liu and P. Y. Li, Synthesis, crystal and electronic structure, anticancer activity of ruthenium(II) arene complexes with thiosemicarbazones, *Appl. Organometal. Chem.*, 2013, **27**, 307–312.

[12] W. Su, Q. Q. Qian, P. Y. Li, X. L. Lei, Q. Xiao, S. Huang, C. S. Huang and J. G. Cui, Synthesis, characterization, and anticancer activity of a series of ketone-N^4-substituted thiosemicarbazones and their ruthenium(II) arene complexes, *Inorg. Chem.*, 2013, **52**, 12440–12449.

[13] P. Hanczyc, P. Lincoln and B. Norden, Interactions of binuclear ruthenium(II) complexes with oligonucleotides in hydrogel matrix: enantioselective threading intercalation into GC context,

J. Phys. Chem. B, 2013, **117**, 2947–2954.

[14] A. Kurzwernhart, W. Kandioller, E. A. Enyedy, M. Novak, M. A. Jakupec, B. K. Keppler and C. G. Hartinger, 3-Hydroxyflavones vs. 3-hydroxyquinolinones: structure–activity relationships and stability studies on RuII(arene) anticancer complexes with biologically active ligands, *Dalton Trans.*, 2013, **42**, 6193–6202.

[15] P. Anitha, N. Chitrapriya, Y. J. Jang and P. Viswanathamurthi, Synthesis, characterization, DNA interaction, antioxidant and anticancer activity of new ruthenium(II) complexes of thiosemicarbazone/semicarbazone bearing 9,10-phenanthrenequinone, *J. Photochem. Photobiol. B*, 2013, **129**, 17–26.

[16] J. Wang, C. Xiang, F. F. Tian, Z. Q. Xu, F. L. Jiang and Y. Liu, Investigating the interactions of a novel anticancer delocalized lipophilic cation and its precursor compound with human serum albumin, *RSC Adv.*, 2014, **4**, 18205–18216.

[17] Y. Zhang, K. Pan and Q. X. Zhong, Characteristics of activated carbon and carbon nanotubes as adsorbents to remove annatto (norbixin) in cheese whey, *J. Agric. Food Chem.*, 2013, **61**, 9230–9240.

[18] Y. Zhang and Q. X. Zhong, Probing the binding between norbixin and dairy proteins by spectroscopy methods, *Food Chem.*, 2013, **139,** 611–616.

[19] X. J. Li, B. L. Zhang, W. Li, X. F. Lei, X. L. Fan, L. Tian, H. P. Zhang and Q. Y. Zhang, Preparation and characterization of bovine serum albumin surface-imprinted thermosensitive magnetic polymer microsphere and its application for protein recognition, *Biosens. Bioelectron.*, 2014, **51**, 261–267.

[20] Q. Xiao, S. Huang, Y. Liu, F. F. Tian and J. C. Zhu, Thermodynamics, conformation and active sites of the binding of Zn-Nd hetero-bimetallic Schiff base to bovine serum albumin, *J. Fluoresc.*, 2009, **19**, 317–326.

[21] O. K. Abou-Zied, Spectroscopy of hydroxyphenyl benzazoles in solution and human serum albumin: detecting flexibility, specificity and high affinity of the warfarin drug binding site, *RSC Adv.*, 2013, **3**, 8747–8755.

[22] Q. Xiao, S. Huang, Z. D. Qi, B. Zhou, Z. K. He and Y. Liu, Conformation, thermodynamics and stoichiometry of HSA adsorbed to colloidal CdSe/ZnS quantum dots, *BBA-Proteins Proteom.*, 2008, **1784**, 1020–1027.

[23] Q. Xiao, S. Huang, W. Su, P. Y. Li, J. Q. Ma, F. P. Luo, J. Chen and Y. Liu, Systematically investigations of conformation and thermodynamics of HSA adsorbed to different sizes of CdTe quantum dots, *Colloids Surf. B*, 2013, **102**, 76–82.

[24] D. W. Li, H. He, B. B. Lin, Z. Q. Xu, F. L. Jiang and Y. Liu, Studies on the isolated mitochondrial damage induced by α-tocopheryl succinate and its interactions with human serum albumin, *RSC Adv.*, 2013, **4**, 3913–3919.

[25] Y. P. Zhang, M. K. Nie, S. Y. Shi, Q. P. You, J. F. Guo and L. L. Liu, Integration of magnetic solid phase fishing and off-line two-dimensional high-performance liquid chromatography–diode array detector–mass spectrometry for screening and identification of human serum albumin binders from Radix Astragali, *Food Chem.*, 2014, **146**, 56–64.

[26] X. R. Li, D. J. Chen, G. K. Wang and Y. Lu, Study of interaction between human serum albumin and three antioxidants: Ascorbic acid, a-tocopherol, and proanthocyanidins, *Eur. J. Med. Chem.*, 2013, **70**, 22–36.

[27] G. J. Zhang, B. Keita, C. T. Craescu, S. Miron, P. D. Oliveira and L. Nadjo, Polyoxometalate binding to human serum albumin: a thermodynamic and spectroscopic approach, *J. Phys. Chem. B*, 2007, **111**, 11253–11259.

[28] A. C. Dong, P. Huang and W. S. Caughey, Protein secondary structures in water from second-derivative amide I infrared spectra, *Biochemistry*, 1990, **29**, 3303–3308.

[29] B. T. Yin, C. Y. Yan, X. M. Peng, S. L. Zhang, S. Rasheed, R. X. Geng and C. H. Zhou, Synthesis and biological evaluation of a-triazolyl chalcones as a new type of potential antimicrobial agents and their interaction with calf thymus DNA and human serum albumin, *Eur. J. Med. Chem.*, 2014, **71**, 148–159.

[30] Q. Xiao, H. N. Qiu, S. Huang, C. S. Huang, W. Su, B. Q. Hu and Y. Liu, Systematic investigation of interactions between papain and MPA-capped CdTe quantum dots, *Mol. Biol. Rep.*, 2013, **40**, 5781–5789.

[31] Q. Xiao, S. Huang, J. Q. Ma, W. Su, P. Y. Li, J. G. Cui and Y. Liu, Systematically investigation of interactions between BSA and different charge-capped CdSe/ZnS quantum dots, *J. Photochem. Photobiol. A*, 2013, **249**, 53–60.

[32] J. R. Lakowicz, Principles of fluorescence spectroscopy 3rd ed., Springer, New York, 2006.

[33] V. P. Bogoeva, M. A. Radeva, L. Y. Atanasova, S. R. Stoitsova and R. N. Boteva,

Fluorescence analysis of hormone binding activities of wheat germ agglutinin, *Biochim. Biophys. Acta*, 2004, **1698**, 213–218.

[34] M. A. Jhonsi, A. Kathiravan and R. Renganathan, Spectroscopic studies on the interaction of colloidal capped CdS nanoparticles with bovine serum albumin, *Colloids Surf. B*, 2009, **72**, 167−172.

[35] C. J. Wilson and R. A. Copeland, Spectroscopic characterization of arrestin interactions with competitive ligands: study of heparin and phytic acid binding, *J. Protein. Chem.*, 1997, **16**, 755–763.

[36] C. B. Murphy, Y. Zhang, T. Troxler, V. Ferry, J. J. Martin and W. E. Jones, Probing Förster and Dexter energy-transfer mechanisms in fluorescent conjugated polymer chemosensors, *J. Phys. Chem. B*, 2004, **108**, 1537–1543.

[37] R. M. Watt and E. W. Voss, Solvent perturbation of the fluorescence of fluorescein bound to specific antibody, *J. Biol. Chem.*, 1979, **254**, 1684–1690.

[38] D. Leckband, Measuring the forces that control protein interactions, *Annu. Rev. Biophys. Biomol. Struct.*, 2000, **29**, 1−26.

[39] D. P. Ross and S. Subramanian, Thermodynamics of protein association reactions: forces contributing to stability, *Biochemistry*, 1981, **20**, 3096–3102.

[40] Y. J. Hu, Y. Liu, W. Jiang, R. M. Zhao and S. S. Qu, Fluorometric investigation of the interaction of bovine serum albumin with surfactants and 6-mercaptopurine, *J. Photochem. Photobiol. B*, 2005, **80**, 235–242.

[41] S. F. Sun, B. Zhou, H. N. Hou, Y. Liu and G. Y. Xiang, Studies on the interaction between Oxaprozin-E and bovine serum albumin by spectroscopic methods, *Int. J. Biol. Macromol.*, 2006, **39**, 197–200.

[42] Y. Li, W. Y. He, J. Q. Liu, F. L. Sheng, Z. D. Hu and X. G. Chen, Binding of the bioactive component Jatrorrhizine to human serum albumin, *Biochim. Biophys. Acta*, 2005, **1722**, 15–21.

[43] D. E. Epps, T. J. Raub and F. J. Kézdy, A general wide-range spectrofluorometric method for measuring the site-specific affinities of drugs toward human serum albumin, *Anal. Biochem.*, 1995, **227**, 342–350.

[44] Y. J. Hu, Y. Liu and X. H. Xiao, Investigation of the interaction between berberine and human

serum albumin, *Biomacromolecules*, 2009, **10**, 517–521.

[45] V. T. G. Chuang and M. Otagiri, Stereoselective binding of human serum albumin, *Chirality*, 2006, **18**, 159–166.

[46] T. Peters Jr., All About Albumin: Biochemistry, Genetics and Medical Applications, Academic Press, San Diego, 1996.

[47] C. Long, E. J. King and W. M. Sperry, Biochemists' Handbook, E. & F. N. Spon Ltd, London, 1961.

[48] B. Valeur, Molecular Fluorescence: Principles and Applications, Wiley Press, New York, 2001.

[49] P. F. Qin, R. T. Liu, X. R. Pan, X. Y. Fang and Y. Mou, Impact of carbon chain length on binding of perfluoroalkyl acids to bovine serum albumin determined by spectroscopic methods, *J. Agric. Food Chem.*, 2010, **58**, 5561–5567.

[50] F. Samari, B. Hemmateenejad, M. Shamsipur and M. Rashidi, Affinity of two novel five-coordinated anticancer Pt(II) complexes to human and bovine serum albumins: a spectroscopic approach, *Inorg. Chem.*, 2012, **51**, 3454–3464.

[51] S. R. Feroz, S. B. Mohamad, N. Bujang, S. N. A. Malek and S. Tayyab, Multispectroscopic and molecular modeling approach to investigate the interaction of flavokawain B with human serum albumin, *J. Agric. Food Chem.*, 2012, **60**, 5899–5908.

[52] G. W. Zhang, L. Wang and J. H. Pan, Probing the binding of the flavonoid diosmetin to human serum albumin by multispectroscopic techniques, *J. Agric. Food Chem.*, 2012, **60**, 2721–2729.

[53] Z. X. Lu, T. Cui and Q. L. Shi, Application of circular dichroism and optical rotatory dispersion in molecular biology, 1st ed., Science Press, Beijing, 1987, 79–82.

[54] S. Li, Y. Z. Wang, J. G. Jiang and S. J. Dong, pH-Dependent protein conformational changes in albumin: gold nanoparticle bioconjugates: a spectroscopic study, *Langmuir*, 2007, **23**, 2714–2721.

[55] Z. Y. Chen, H. Y. Xu, Y. L. Zhu, J. Y. Liu, K. Y. Wang, P. X. Wang, S. J. Shang, X. N. Li, Z. L. Wang, W. Shao and S. D. Zhang, Understanding the fate of an anesthetic, nalorphine upon interaction with human serum albumin: a photophysical and mass-spectroscopy approach, *RSC Adv.*, 2014, **4**, 25410−25419.

[56] S. Huang, F. W. Zhu, H. N. Qiu, Q. Xiao, Q. Zhou, W. Su and B. Q. Hu, A sensitive quantum dots-based "OFF-ON" fluorescent sensor for ruthenium anticancer drugs and ctDNA, *Colloids Surf. B*, 2014, **117**, 240−247.

[57] J. Zhang, R. Li, F. L. Jiang, B. Zhou, Q. Y. Luo, Q. L. Y. Yu, X. L. Han, Y. Lin, H. He, Y. Liu and Y. L. Wang, An electrochemical and surface plasmon resonance study of adsorption actions of DNA by Escherichia coli, *Colloids Surf. B*, 2014, **117**, 68−74.

Table 1. Stern–Volmer quenching constants K_{SV}, bimolecular quenching constants k_q, modified Stern–Volmer association constants K_a and relative thermodynamic parameters for the interaction between the anticancer drug and HSA at three different temperatures.

Table 2. The binding constants K_b and binding numbers n at different temperatures.

Table 3. The binding constants K_b of drug–HSA system at 298 K in the presence of some common ions.

Table 4. Three-dimensional fluorescence spectral characteristics of HSA and drug–HSA system.

Table 5. Fractions of different secondary structures determined by SELCON3

Figure Captions

Fig. 1. Emission spectra of HSA in the presence of various concentrations of this anticancer drug. (pH 7.4, T = 298 K, λ_{ex} = 295 nm). The insert corresponds to the Stern–Volmer plot of HSA with the increasing concentration of this anticancer drug at 298 K. c (HSA) = 2.0 × 10^{-6} mol L^{-1}; c (drug) / (10^{-6} mol L^{-1}), 1-11: 0; 0.1; 0.2; 0.3; 0.4; 0.5; 0.6; 0.7; 0.8; 0.9; 1.0; curve L shows the emission spectrum of this anticancer drug only, c (drug) = 1.0 × 10^{-6} mol L^{-1}.

Fig. 2. The Stern–Volmer plots of drug–HSA system (A) and the modified Stern-Volmer plots of drug–HSA system (B) at three different temperatures.

Fig. 3. UV-visible spectra of HSA in the presence of this anticancer drug. (A) The absorption spectrum of this anticancer drug only; (B) the absorption spectrum of HSA only; (C) The absorption spectrum of drug–HSA system when the mole ratio is 1:1; (D) the difference absorption spectrum between drug–HSA system and drug at the same concentration. c (HSA) = c (drug) = 2.0 × 10^{-6} mol L^{-1}.

Fig. 4. Van't Hoff plots of drug–HSA system.

Fig. 5. Effect of site-specific probe to drug–HSA system, (A) warfarin; (B) ibuprofen (pH 7.4, T = 298 K, λ_{ex} = 295 nm). (C) The modified Stern-Volmer plots of drug–HSA system alone and with warfarin or ibuprofen probe. c (warfarin) = c (ibuprofen) = c (HSA) = 2.0 × 10^{-6} mol L^{-1}; c (drug) / (10^{-6} mol L^{-1}), 1-11: 0; 0.1; 0.2; 0.3; 0.4; 0.5; 0.6; 0.7; 0.8; 0.9;1.0; The inserts correspond to the molecular structures of site-specific probe.

Fig. 6. Overlapping between the UV-vis absorption spectrum of this anticancer drug (a) and the fluorescence emission spectrum of HSA (b) (λ_{ex} = 295 nm). *c* (HSA) = *c* (drug) = 2.0×10^{-6} mol L^{-1}.

Fig. 7. Synchronous fluorescence spectrum of drug–HSA system, (A) $\Delta\lambda$ = 15 nm; (B) $\Delta\lambda$ = 60 nm. (C) Quenching of HSA synchronous fluorescence by this anticancer drug. *c* (HSA) = 2.0×10^{-6} mol L^{-1}; *c* (drug) / (10^{-6} mol L^{-1}); 1-13: 0; 0.4; 0.8; 1.2; 1.6; 2.0; 2.4; 2.8; 3.2; 3.6; 4.0; 4.4; 4.8.

Fig. 8. Three-dimensional fluorescence spectra of HSA alone (A) and drug–HSA system (B).

Fig. 9. ATR FT-IR spectra of HSA and drug–HSA system in PBS of pH 7.4 solution: (A) FT-IR spectrum of HSA only; (B) FT-IR spectra of drug–HSA system. All the spectra spanned the 1800–1450 cm^{-1} regions.

Fig. 10. The CD spectra of the drug–HSA system obtained in 0.1 mol L^{-1} PBS of pH 7.4 at room temperature. The concentration of HSA was fixed at 2.0×10^{-6} mol L^{-1} (a). In drug–HSA system, the concentrations of this anticancer drug were 2.0×10^{-6} mol L^{-1} (b), 6.0×10^{-6} mol L^{-1} (c), 1.0×10^{-5} mol L^{-1} (d) and 1.4×10^{-5} mol L^{-1} (e), respectively.

Fig. 11. The mass spectra of anticancer drug alone (A), HSA alone (B), the drug–HSA system with molar ratio of 1:1 (C) and 2:1 (D), respectively.

Fig. 12. Cyclic voltammograms of bare Au electrode and HSA-modified Au electrode in the absence and the presence of various concentrations of this anticancer drug. *c* (drug) / (10^{-7} mol L^{-1}); 1-9: 0, 1.2, 2.4, 3.6, 4.8, 6.0, 7.2, 8.4, 9.6. Insert was the linear relationship existed between the reciprocal of the current drop and the reciprocal of this anticancer drug concentration in this range.

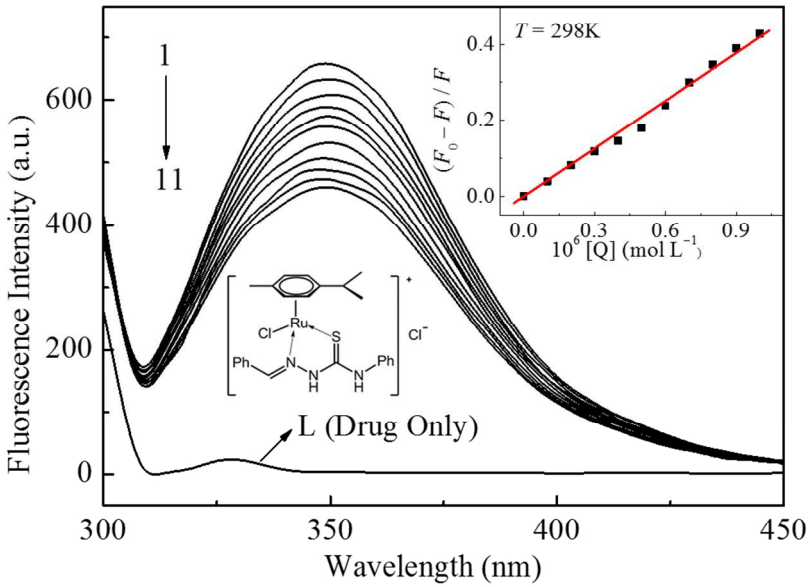

Fig. 1. Emission spectra of HSA in the presence of various concentrations of this anticancer drug. (pH 7.4, T = 298 K, λex = 295 nm). The insert corresponds to the Stern–Volmer plot of HSA with the increasing concentration of this anticancer drug at 298 K. c (HSA) = 2.0 × 10–6 mol L–1; c (drug) / (10–6 mol L–1), 1-11: 0; 0.1; 0.2; 0.3; 0.4; 0.5; 0.6; 0.7; 0.8; 0.9; 1.0; curve L shows the emission spectrum of this anticancer drug only, c (drug) = 1.0 × 10–6 mol L–1.
208x145mm (150 x 150 DPI)

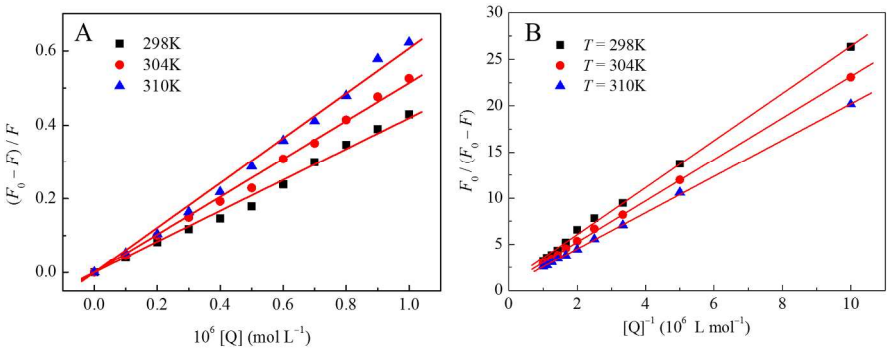

Fig. 2. The Stern–Volmer plots of drug–HSA system (A) and the modified Stern-Volmer plots of drug–HSA system (B) at three different temperatures.
377x146mm (150 x 150 DPI)

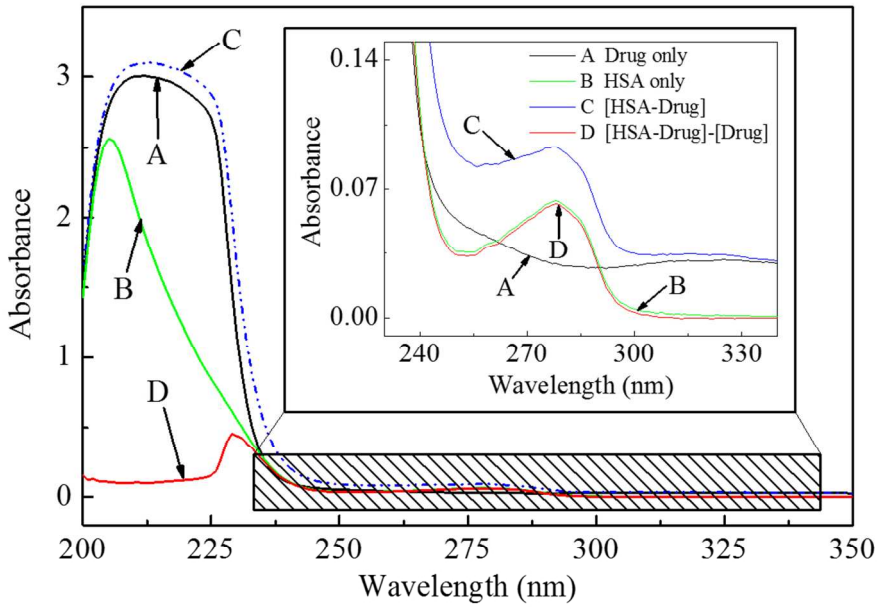

Fig. 3. UV-visible spectra of HSA in the presence of this anticancer drug. (A) The absorption spectrum of this anticancer drug only; (B) the absorption spectrum of HSA only; (C) The absorption spectrum of drug–HSA system when the mole ratio is 1:1; (D) the difference absorption spectrum between drug–HSA system and drug at the same concentration. c (HSA) = c (drug) = 2.0 × 10–6 mol L–1.
208x146mm (150 x 150 DPI)

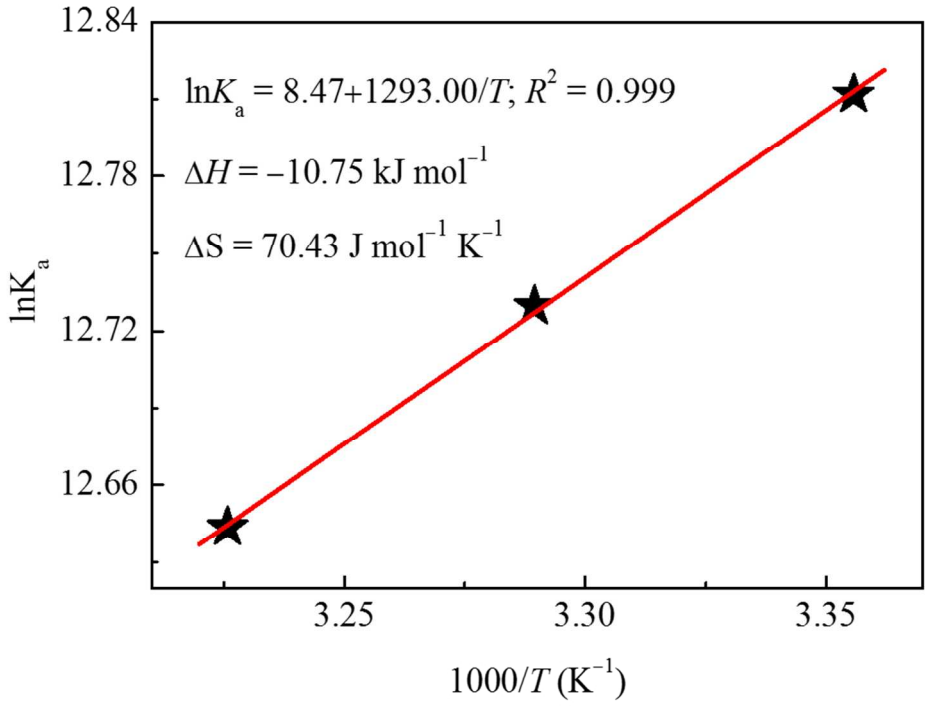

Fig. 4. Van't Hoff plots of drug–HSA system.
181x141mm (150 x 150 DPI)

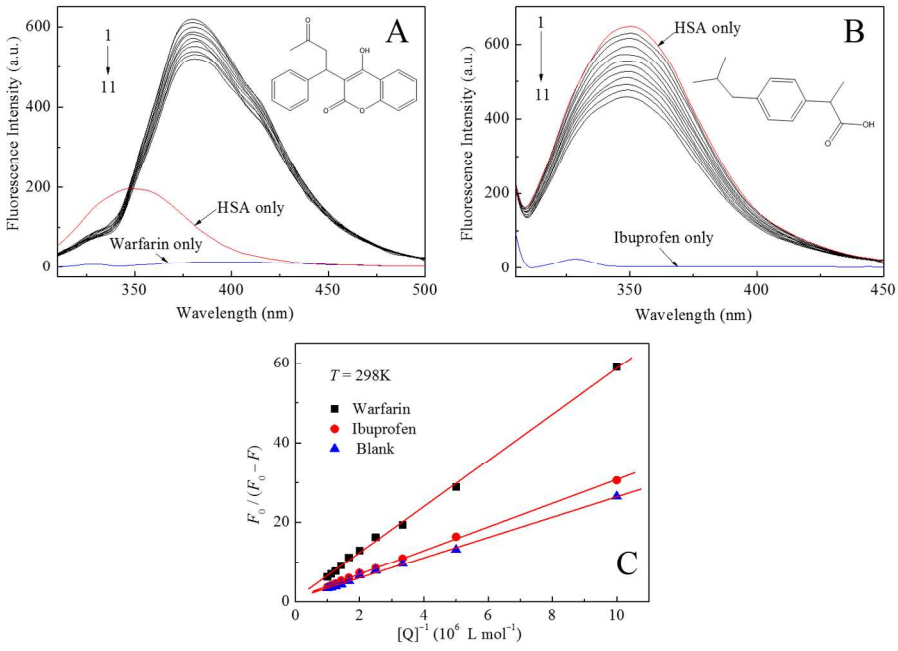

Fig. 5. Effect of site-specific probe to drug–HSA system, (A) warfarin; (B) ibuprofen (pH 7.4, T = 298 K, λex = 295 nm). (C) The modified Stern-Volmer plots of drug–HSA system alone and with warfarin or ibuprofen probe. c (warfarin) = c (ibuprofen) = c (HSA) = 2.0 × 10–6 mol L–1; c (drug) / (10–6 mol L–1), 1-11: 0; 0.1; 0.2; 0.3; 0.4; 0.5; 0.6; 0.7; 0.8; 0.9;1.0; The inserts correspond to the molecular structures of site-specific probe.
291x204mm (150 x 150 DPI)

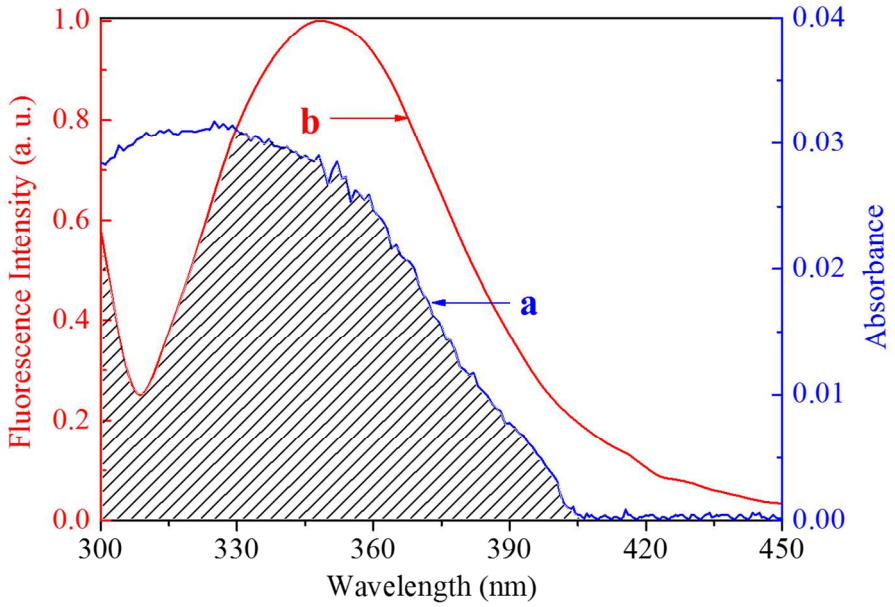

Fig. 6. Overlapping between the UV-vis absorption spectrum of this anticancer drug (a) and the fluorescence emission spectrum of HSA (b) (λex = 295 nm). c (HSA) = c (drug) = 2.0 × 10–6 mol L–1.
239x168mm (150 x 150 DPI)

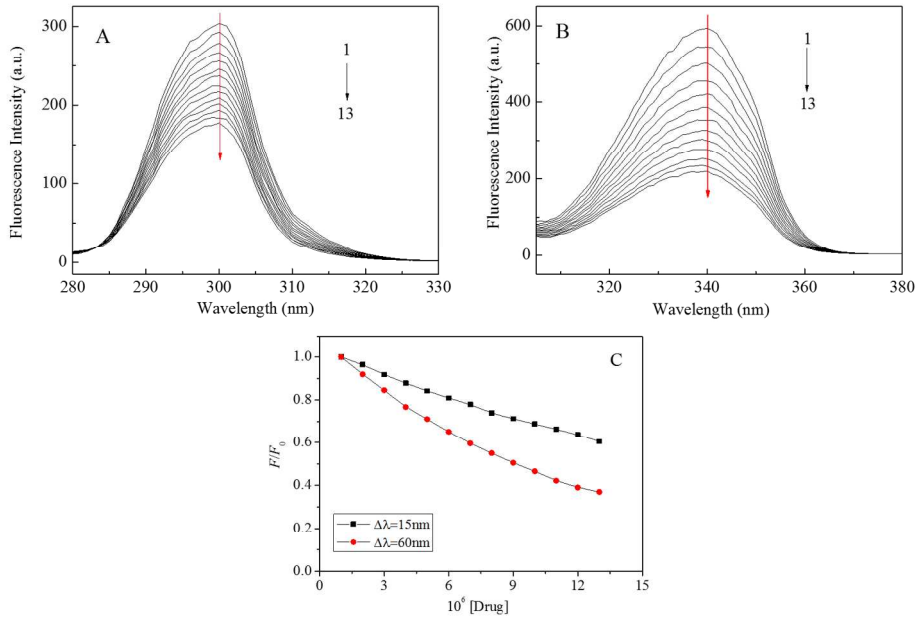

Fig. 7. Synchronous fluorescence spectrum of drug–HSA system, (A) Δλ = 15 nm; (B) Δλ = 60 nm. (C) Quenching of HSA synchronous fluorescence by this anticancer drug. c (HSA) = 2.0 × 10–6 mol L–1; c (drug) / (10–6 mol L–1); 1-13: 0; 0.4; 0.8; 1.2; 1.6; 2.0; 2.4; 2.8; 3.2; 3.6; 4.0; 4.4; 4.8.
312x207mm (150 x 150 DPI)

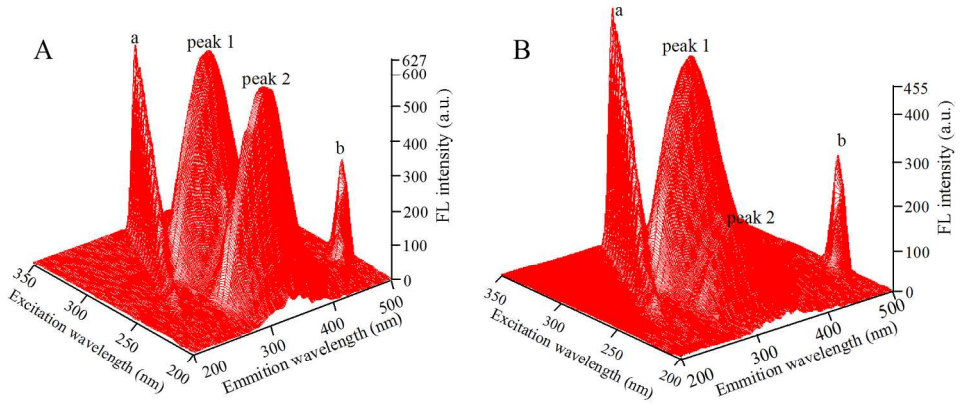

Fig. 8. Three-dimensional fluorescence spectra of HSA alone (A) and drug–HSA system (B).
355x169mm (150 x 150 DPI)

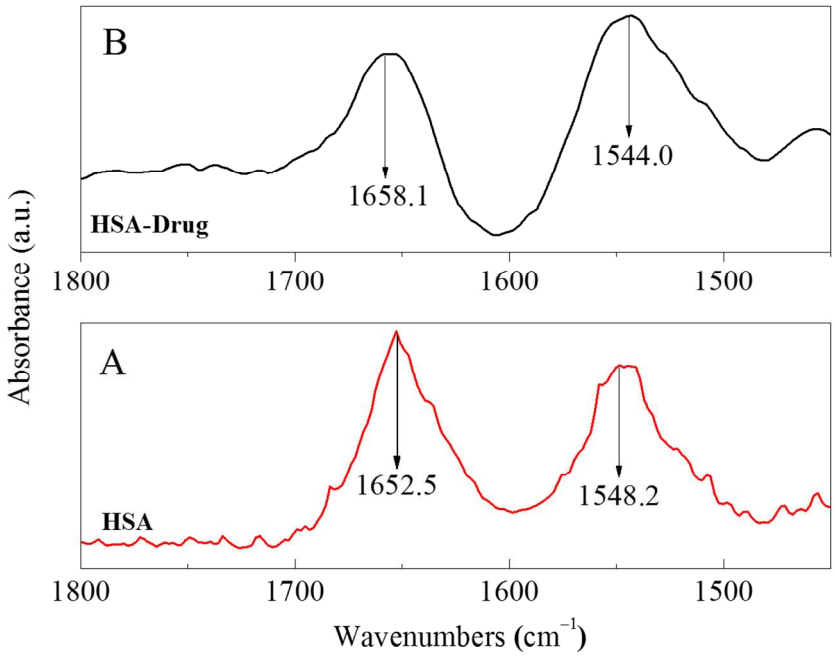

Fig. 9. ATR FT-IR spectra of HSA and drug–HSA system in PBS of pH 7.4 solution: (A) FT-IR spectrum of HSA only; (B) FT-IR spectra of drug–HSA system. All the spectra spanned the 1800–1450 cm−1 regions.
239x168mm (150 x 150 DPI)

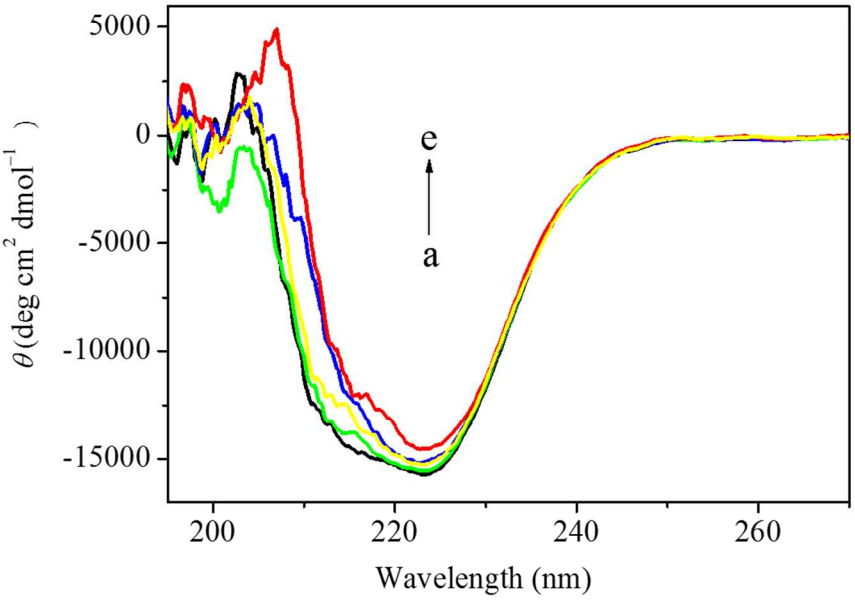

Fig. 10. The CD spectra of the drug–HSA system obtained in 0.1 mol L–1 PBS of pH 7.4 at room temperature. The concentration of HSA was fixed at 2.0 × 10−6 mol L–1 (a). In drug–HSA system, the concentrations of this anticancer drug were 2.0 × 10−6 mol L–1 (b), 6.0 × 10−6 mol L–1 (c), 1.0 × 10−5 mol L–1 (d) and 1.4 × 10−5 mol L–1 (e), respectively.
210x145mm (150 x 150 DPI)

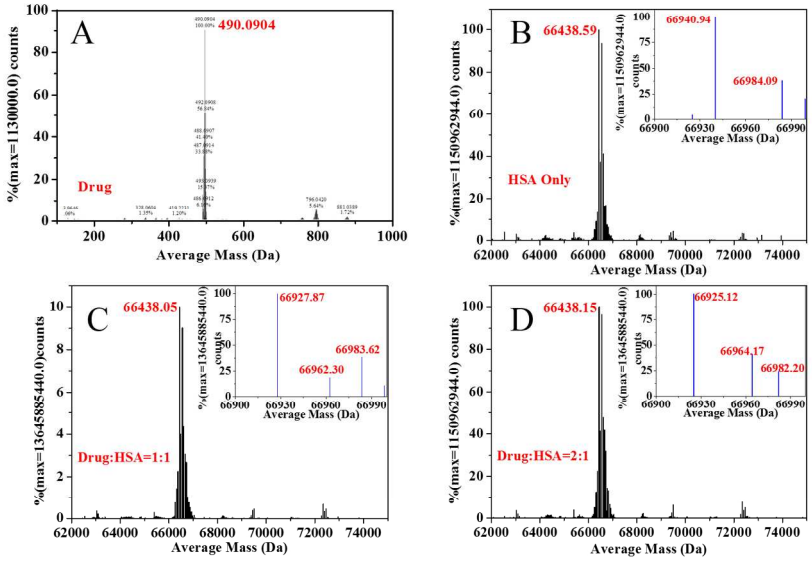

Fig. 11. The mass spectra of anticancer drug alone (A), HSA alone (B), the drug–HSA system with molar ratio of 1:1 (C) and 2:1 (D), respectively.
339x228mm (150 x 150 DPI)

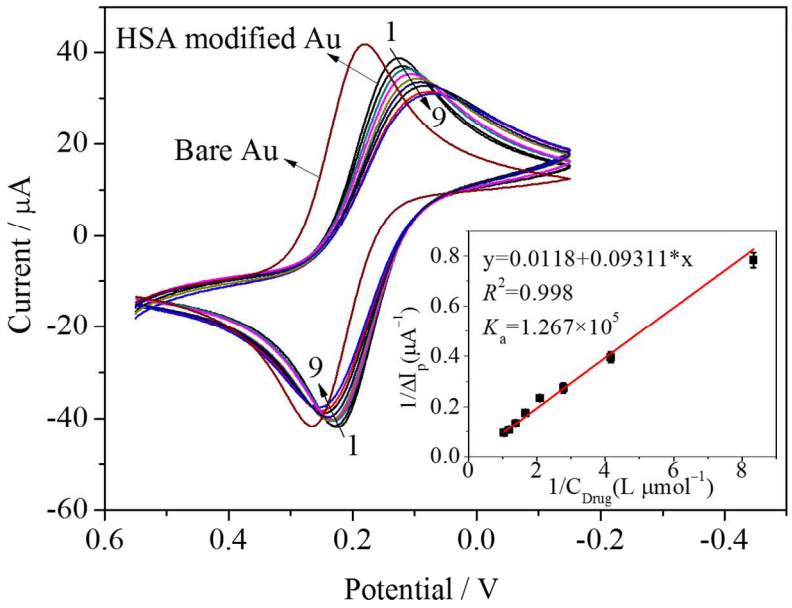

Fig. 12. Cyclic voltammograms of bare Au electrode and HSA-modified Au electrode in the absence and the presence of various concentrations of this anticancer drug. c (drug) / (10–7 mol L–1); 1-9: 0, 1.2, 2.4, 3.6, 4.8, 6.0, 7.2, 8.4, 9.6. Insert was the linear relationship existed between the reciprocal of the current drop and the reciprocal of this anticancer drug concentration in this range.
258x181mm (150 x 150 DPI)

Table 1. Stern–Volmer quenching constants K_{SV}, bimolecular quenching constants k_q, modified Stern–Volmer association constants K_a and relative thermodynamic parameters for the interaction between the anticancer drug and HSA at three different temperatures.

pH	T / (K)	K_{sv} (10^5 L mol^{-1})	K_q (10^{13} L mol^{-1} s^{-1})	R^{2a}	*S.D.*[b]	K_a (10^5 L mol^{-1})	R^{2a}	ΔH (kJ mol^{-1})	ΔG (kJ mol^{-1})	ΔS (J mol^{-1} K^{-1})	R^{2a}	*S.D.*[b]
	298	4.19	4.19	0.996	0.014	3.67	0.998		–31.74			
7.4	304	5.14	5.14	0.998	0.012	3.38	0.999	–10.75	–32.17	70.43	0.999	0.012
	310	6.07	6.07	0.997	0.017	3.10	0.999		–32.58			

[a] R^2 is the correlation coefficient;
[b] *S.D.* is standard deviation.

Table 2. The binding constants K_b and binding numbers n at different temperatures.

pH	T / (K)	K_b (10^5 L mol^{-1})	n	R^{2a}	$S.D.$[b]
7.4	298	7.16	1.08	0.996	0.028
	304	10.62	1.05	0.998	0.017
	310	21.74	1.09	0.999	0.013

[a] R^2 is the correlation coefficient;
[b] *S.D.* is standard deviation.

Table 3. The binding constants K_b of drug–HSA system at 298 K in the presence of some common ions.

Systems	K_b (10^5 L mol^{-1})	n	R^a	$S.D.^b$	$K / K_0{}^c$
drug–HSA	7.16	1.09	0.996	0.028	1
drug–HSA–Ag^+	1.76	0.96	0.998	0.019	0.247
drug–HSA–K^+	5.99	1.05	0.999	0.012	0.837
drug–HSA–Na^+	7.67	1.07	0.999	0.014	1.071
drug–HSA–Cu^{2+}	2.93	0.99	0.999	0.012	0.409
drug–HSA–Zn^{2+}	6.27	1.06	0.999	0.015	0.875
drug–HSA–Ca^{2+}	3.80	1.02	0.998	0.018	0.532
drug–HSA–Mg^{2+}	8.57	1.07	0.997	0.012	1.197
drug–HSA–Ni^{2+}	1.07	0.93	0.999	0.027	0.150
drug–HSA–Co^{2+}	6.47	1.06	0.999	0.013	0.904
drug–HSA–NO_3^-	1.76	0.97	0.998	0.019	0.247
drug–HSA–SO_4^{2-}	2.93	0.99	0.999	0.012	0.409
drug–HSA–Cl^-	1.07	0.93	0.999	0.027	0.150

[a] R^2 is the correlation coefficient;
[b] *S.D.* is standard deviation;
[c] K_0 and K are the apparent binding constants of drug–HSA system alone and drug–HSA system in the absence of metal ion, respectively.

Table 4. Three-dimensional fluorescence spectral characteristics of HSA and drug–HSA system.

Peaks	HSA			drug–HSA system		
	Peak position $\lambda_{ex/em}$ (nm/nm)	Stokes shift $\Delta\lambda$ (nm)	Intensity F	Peak position $\lambda_{ex/em}$ (nm/nm)	Stokes shift $\Delta\lambda$ (nm)	Intensity F
Fluorescence peak 1	285.0/346.6	61.6	627.5	285.0/346.1	61.1	438.2
Fluorescence peak 2	230.0/345.9	115.9	614.4	245.0/349.4	104.4	158.3

Table 5. Fractions of different secondary structures determined by SELCON3

Concentration of the anticancer drug (mol L^{-1})	percentage of secondary structure					
	α-helix		β-strand		turn	unordered
	α_R	α_D	β_R	β_D		
0	42.2	17.9	3.1	2.9	13.8	20.1
2.0×10^{-6}	38.8	17.2	3.5	3.2	15.2	22.1
6.0×10^{-6}	35.7	16.6	3.8	3.4	18.1	22.4
1.0×10^{-5}	31.2	15.4	4.0	3.8	22.1	23.5
1.4×10^{-5}	28.5	14.9	4.2	4.0	23.6	24.8

The subscripts “R” and “D” represent “ordered” and “disordered”, respectively.